metals

MDPI

Article

Control of the Lamellar Structure and Analysis of Tensile Properties of TiC/Ti-6Al-3Sn-9Zr-1.5Mo Composite Produced by In Situ Casting Technique

Dongdong Zhu [1], Duo Dong [1,*], Li Liu [1], Xiaohong Wang [1] and Jiqiu Qi [2,*]

[1] Key Laboratory of Air-Driven Equipment Technology of Zhejiang Province, Quzhou University, Quzhou 324000, China; zhudd8@163.com (D.Z.); li_liull@163.com (L.L.); hitxiaohong_wang@hotmail.com (X.W.)
[2] School of Materials and Physics, China University of Mining and Technology, Xuzhou 221116, China
* Correspondence: dongduohit@163.com (D.D.); qijiqiu@cumt.edu.cn (J.Q.); Tel.: +86-516-8359-1788 (D.D.)

Abstract: In the present paper, new heat treatment was performed on 10 vol.% TiC/Ti-6Al-3Sn-9Zr-1.5Mo composite fabricated by an in situ casting technique. The aim is to obtain fully lamellar structure in matrix, control the lamellar structure quantitatively and understand the variation of the tensile properties of as-cast and heat-treated composites. For as-cast composite, matrix exhibited fully lamellar structure with some extent of basket-weave characteristics, and reinforcement was mainly in fine rod and strip shape. After β heat treatment, matrix microstructure was refined visibly. As the new cooling method was employed, wider α lath in matrix was obtained. The composite with very fine lamellar structure showed better yield strength (YS) in comparison with that with coarse lamellar microstructure below 650 °C. At 700 °C, fine grain strengthening cannot exert effective influence on tensile strength. It is proved that the enhanced YS is mainly ascribed to the refinement of α lath at ambient temperature. The heat-treated composites with wider α lath displayed excellent ductility at ambient temperature. Above 600 °C, the effect of α phase size on tensile elongation was negligible in the heat-treated composites, since matrix was softened.

Keywords: titanium matrix composite; lamellar microstructure; tensile properties; heat treatment; TiC

Citation: Zhu, D.; Dong, D.; Liu, L.; Wang, X.; Qi, J. Control of the Lamellar Structure and Analysis of Tensile Properties of TiC/Ti-6Al-3Sn-9Zr-1.5Mo Composite Produced by In Situ Casting Technique. *Metals* **2021**, *11*, 160. https://doi.org/10.3390/met11010160

Received: 10 December 2020
Accepted: 13 January 2021
Published: 16 January 2021

1. Introduction

Discontinuously reinforced titanium matrix composites (TMCs) have been considered as a promising material for aerospace application because of their high strength and excellent wear resistance at elevated temperatures [1–3]. TiC particle-reinforced TMCs (TiC-TMCs) have been reported extensively, since TiC particles possess the excellent balance of stability, stiffness, modulus and compatibility with Ti matrices [4–7]. In the past few decades, in situ synthesized technique and traditional casting has been combined to produce TMCs owing to its obvious advantages such as simplicity, low cost, direct casting forming and large-scale production [8–12].

Much work has indicated that the influence of matrix microstructures on mechanical properties of TMCs is significant, especially at low temperatures [13–15]. Generally, the lamellar microstructure, equiaxed microstructure and duplex microstructure can be obtained in titanium alloys and TMCs through heat treatment or other methods [16,17]. Wang et al. [18] pointed out that TMCs with fully lamellar structure display superior comprehensive properties in comparison with those with equiaxed structure. Furthermore, lamellar microstructure can more effectively impede the propagation of cracks generating in cracked reinforcements. Qi et al. [19] also obtained similar results in TiC-TMCs. Hence, in order to produce TMCs castings with high tensile properties, the lamellar microstructure should be selected. It is well established that lamellar microstructure is formed during cooling from above the β-transus temperature in TMCs [20–24]. Therefore, only the cool-

ing process is controlled; α phase size in the lamellar microstructure can be controlled quantitatively. However, little work has been done to control this process in cast TMCs.

In this paper, 10 vol.% TiC/Ti-6Al-3Sn-9Zr-1.5Mo composite was prepared by using an in situ casting route, and a new heat treatment was exploited and conducted on this composite. The main purpose of this experimental study was to control lamellar structure quantitatively and analyze the tensile properties of the composite.

2. Materials and Methods

2.1. Preparation of the Composite

The raw material used in this experiment for fabricating 10 vol.% TiC/Ti-6Al-3Sn-9Zr-1.5Mo were pure titanium (99.9 wt.%), high purity aluminum (99.99 wt.%), Sn (99.9 wt.%), zirconium sponge (99.4 wt.%), Al-9 wt.% Mo master alloy and C powder. This composite was melted by induction melting furnace. The temperature of the melt reached about 2000 °C during the induction melting step. Before induction heating starts, the melting chamber was vacuumized and its vacuum degree is lower than 10^{-1} Pa; subsequently, argon backfilled into the chamber. When the raw materials were completely melted, in order to ensure chemical homogeneity, the composite melt was kept at molten state and electromagnetic stirring condition for about 5 min. Finally, the composite melt was cast into a machined graphite mold to form flake composite casting with a length, height and thickness of 200, 200 and 12 mm, respectively.

2.2. Heat Treatment Process

Samples for microstructure analysis and tensile tests were cut from the composite casting. A metallographic technique was used to measure the β-transus temperature of the composite. First, the specimens were heated to a temperature that is much higher than β-transus temperature and then were held for about 1h. Second, several target temperatures, which are near β-transus temperature, with 5 °C intervals were chosen. The fully β phase samples were cooled to the target temperatures and held for 30 min, then quenched. If no α phase is observed, the target temperature is higher than β-transus temperature. The β-transus temperature was determined at about 1095 °C. The specimens for heat treatment were all encapsulated in evacuated quartz tubes, and all heated to 1120 °C first and held at this temperature for 8h. Subsequently, some specimens were cooled in air directly. This heat treatment is so-called β heat treatment, referred to as HT1 here. After 1120 °C/8h, some specimens were put in a furnace with a temperature of 450 °C and held for 30 min, referred to as HT2. The remaining specimens were cooled in a furnace with a temperature of 600 °C for 30 min, referred to as HT3.

2.3. Microstructure Examination

Microstructure observations were carried out by optical microscope (OM, Zeiss, Oberkochen, Germany) and FEI Quanta 200F scanning electron microscope (SEM, FEI, Hillsboro, OR, USA). Phase identification was carried out via X-ray diffraction (XRD, Bruker, Billerica, MA, USA) using a Rigaku D/max-RB X-ray diffractometer with monochromatic Cu Ka radiation. The scan step and step time adopted for XRD were 0.04° and 1 s per step, respectively. Image Proplus (Version 6.0) was used to measure TiC volume fraction.

2.4. Tensile Test

Flat tensile specimens with gauge section of 20 × 4 × 2 mm were tested on an Instron 5500R testing machine (Instron, Norwood, MA, USA) at ambient temperature, 600, 650 and 700 °C. The composite specimens were deformed to failure at a strain rate of 0.5 mm/min. For high-temperature tests, the specimens were first heated to the test temperature, held for 5 min and then deformed to failure. At each condition, three tensile specimens were repeated to obtain average values. Hitachi S-570 SEM (SEM, Hitachi, Chiyoda, Japan) was used to examine fracture surfaces of the as-cast and heat-treated composites.

3. Results

3.1. Phase Identification and Microstructure

3.1.1. Phase Identification

The X-ray diffraction pattern of the as-cast composite is illustrated in Figure 1. It can be seen that only two phases can be found in the present composite, which are α-Ti and TiC. The XRD result confirms that the in situ casting technique is feasible to prepare the composite, and TiC is the only carbide, although Zr content reached 9%.

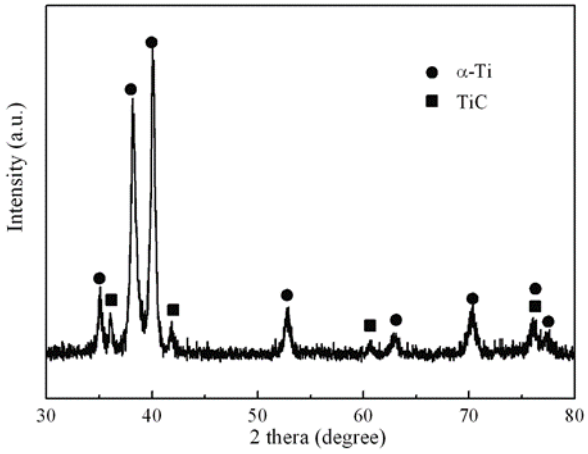

Figure 1. X-ray diffraction patterns of the as-cast composite.

3.1.2. As-Cast Microstructure

Figure 2 displays the characteristics of TiC and matrix in the as-cast composite. Through image analysis of micrograph in Figure 2a, the volume fraction of TiC is approximately 9.4%, very close to the designed value. TiC reinforcements were uniformly distributed in the composite macroscopically, but TiC clusters in some areas were observed (Figure 2a). Microstructural observation showed that TiC mainly grew in fine rod and strip shape (Figure 2a), which is identified as eutectic TiC [25]. Small amounts of TiC exhibited equiaxed or near-equiaxed shape, which corresponds to primary TiC [25]. Research indicated that TiC mainly displays equiaxed or near-equiaxed morphology in 10 vol.% TiC/Ti-6Al-3Sn-3.5Zr-0.4Mo-0.75Nb-0.35Si and 10 vol.% TiC/Ti-6Al-2Zr-1.5Mo-1V composites [19–26]. With the increase in Zr contents to 9% in this study, the volume fraction of primary TiC decreases. It is assumed that increasing Zr content in matrix can promote the precipitation of eutectic TiC. According to Ti-Zr binary phase diagram, Ti and Zr elements can be infinite mutual dissolution. Additionally, with the increase in Zr content, the liquidus temperature of Ti-Zr alloys decreases, which results in the degradation of supercooling degree ahead of the solid–liquid interface. The decrease in supercooling degree inhabits the precipitation of primary TiC. Relatively speaking, the precipitation of eutectic TiC is promoted. Typical fully lamellar structure with some extent of basket-weave characteristic in Figure 2b was formed during the solid-state transformation of $\beta \rightarrow \alpha$. The width of α lath was measured to be about 1.27 μm.

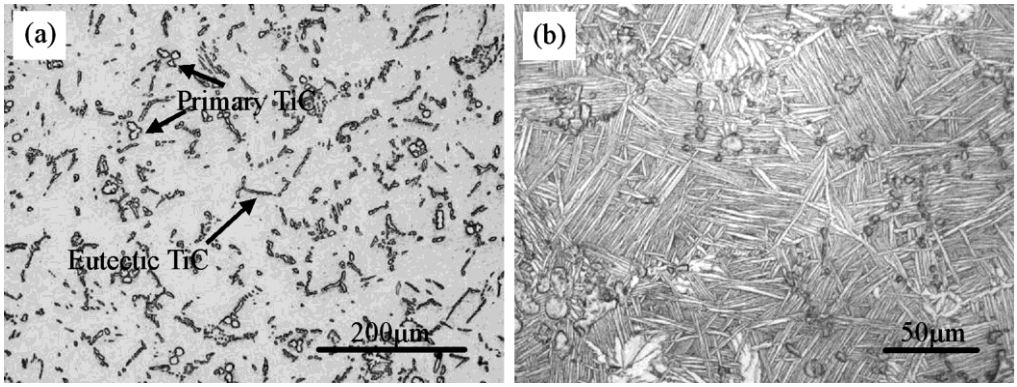

Figure 2. Microstructures of as-cast composite: (**a**) TiC morphology; (**b**) matrix feature.

3.1.3. Heat-Treated Microstructure

Figure 3 exhibits the microstructures of the composite after heat treatment. It can be seen from Figure 3a,b that as HT1 heat treatment was conducted on the composite, significant changes took place in TiC morphology and matrix feature. TiC with fine rod and strip shape almost cannot be observed after HT1 heat treatment, which evolved into equiaxed or near-equiaxed shape (see Figure 3a). It was reported that the spheroidizing of TiC reinforcement during high-temperature heat treatment promotes the formation of equiaxed TiC particles [27]. The reinforcements varied from 1 to 10 μm in diameter, and the average size was 7.2 μm in Figure 3b. Matrix microstructure in the composite via HT1 exhibited lamellar structure with obvious basket-weave characteristic. α phase size was refined remarkably in comparison with that in as-cast microstructure, and the average α lath width is about 0.38 μm.

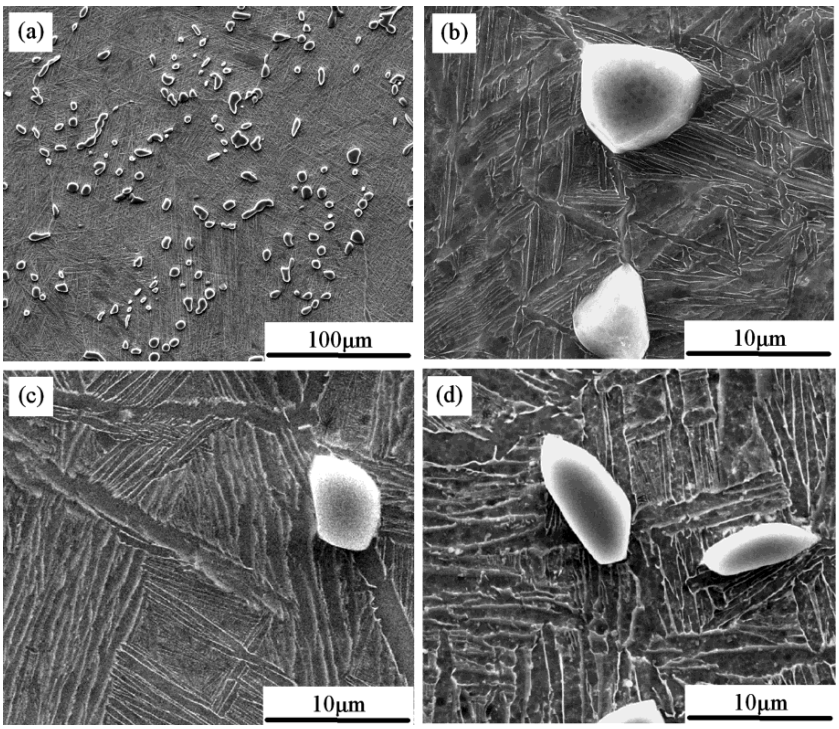

Figure 3. SEM images showing the microstructures of the composite with different heat treatment processes: (**a**,**b**) HT1, (**c**) HT2 and (**d**) HT3.

As the composite was cooled in a special way from β phase region, i.e., the composite was cooled in a furnace with a temperature of 450 °C (HT2), the basic feature in the matrix is similar to that of the composite via HT1, as shown in Figure 3c. However, the basket-weave

feature became unapparent, and the α colony characteristic was more obvious. In addition, the α phase size increased markedly, measured to be 0.78 μm. The only difference between HT1 and HT2 is the cooling method. Apparently, the composite via HT2 was cooled slowly as compared to that via HT1. Increasing cooling rate can enhance the phase transformation rate of $\beta \rightarrow \alpha$. It has been reported that the cooling rate from heat treatment temperature is extremely important, and it determines the final α lamellae size [28]. Rapid cooling from β phase field can lead to the formation of martensite α′ in near-α titanium alloys, and the size of α′ is extremely fine. A decreasing cooling rate favors the generation of typical lamellar microstructure in these alloys, and the lower the cooling rate, the coarser α lath is.

As the composite was cooled in a furnace with higher temperature (600 °C) (HT3), the composite still possesses a fully lamellar structure in matrix (Figure 3d). However, further coarseness in the matrix occurred, and the α lath width measurement was 1.14 μm. It is assumed that further increase in furnace temperature during cooling must further coarse α lamellae. Apparently, α phase size is sensitive to cooling rate, and α lath size can be controlled through controlling the cooling process.

3.2. Tensile Properties

Figure 4 shows the ambient-temperature tensile properties of the composite before and after heat treatment. The results here are the average values obtained from repeated tests. In as-cast composite, the yield strength (YS) and ultimate tensile strength (UTS) are 1041.6 and 1124.2 MPa, respectively, and the tensile elongation is 1.77% (Figure 4). Obviously, UTS of as-cast composite is far higher than YS, indicating that the work hardening rate past yielding is high. As HT1 heat treatment was performed on the composite, YS and UTS are all enhanced evidently, reaching to 1080.8 and 1164.7 MPa, respectively. However, the tensile elongation decreases slightly (Figure 4). After HT2 heat treatment, YS and UTS decrease but ambient-temperature ductility increases compared to those of the composite via HT1. The composite via HT3 exhibits great elongation of 3.56%, although its YS is slightly low. Clearly, heat treatment plays an important role on the ambient-temperature tensile properties of the composite. The degradation of YS is accompanied by the enhancement of elongation after heat treatment (Figure 4).

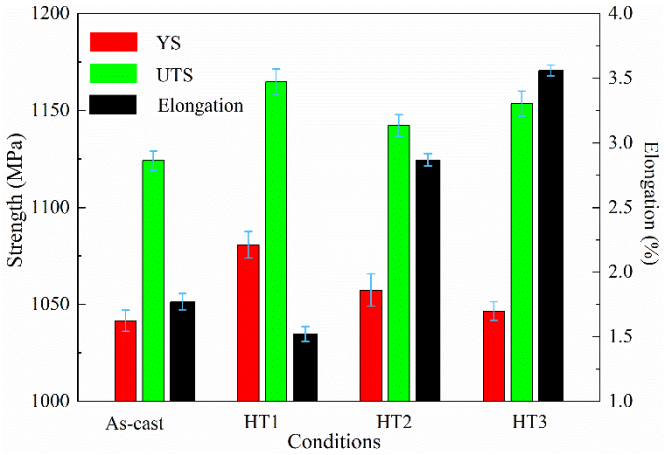

Figure 4. Ambient-temperature tensile properties of the composite before and after heat treatment.

Table 1 summarizes the tensile properties of the as-cast and heat-treated composites at elevated temperatures. At 600 °C, HT1, HT2 and HT3 heat treatments all result in the improvement of UTS, and elongation and the increments in UTS are about 50, 22 and 4 MPa, respectively, in comparison with UTS of as-cast composite. Obviously, the influence of heat treatment on UTS at 600 °C is similar to that at ambient temperature. It is deduced that UTS of the composite at 600 °C is sensitive to α phase size. A further increase in α phase size is believed to cause a further decrease in UTS at 600 °C. Here, the UTS of cast 10 vol.% TiC/Ti-6Al-3Sn-9Zr-1.5Mo composite via HT1 heat treatment approaches 797.6 MPa at

600 °C. Research indicated that as traditional high-temperature titanium alloy was selected as matrix, the UTS of the cast composite is only 660.1 MPa at 600 °C. It can be deduced that increasing Zr content in matrix can effectively improve high-temperature UTSs of TMCs.

Table 1. Elevated-temperature tensile properties of the as-cast and heat-treated composites.

Conditions	600 °C		650 °C		700 °C	
	UTS (MPa)	Elongation (%)	UTS (MPa)	Elongation (%)	UTS (MPa)	Elongation (%)
As-cast	747.3	4.47	635.4	8.43	463.6	13.05
HT1	797.6	5.02	649.2	10.62	462.1	15.15
HT2	769.6	5.88	639.5	10.20	462.4	14.26
HT3	751.1	6.53	637.4	9.26	459.5	13.86

As the temperature increases to 650 °C, UTS decreases but elongation increases observably and the discrepancy in UTSs of as-cast and heat-treated composites becomes small compared to that at 600 °C (Table 1). With a further increase in temperature, a further decrease in UTS is observable and more importantly, the UTS and elongation of the composite before and after heat treatment are almost at the same level, respectively (see Table 1).

3.3. Fractography

SEM fractography of the as-cast and heat-treated composites tested at ambient temperature are shown in Figure 5. It can be seen from Figure 5 that the fracture surfaces are relatively rough when viewed on a microscopic scale. On the facture surface of the as-cast composite, fractured TiC particles with relative smooth facet characteristics and tearing ridges of cracked matrix were observable in Figure 5a. Additionally, it was found that there existed secondary cracks in some fractured TiC particles, indicating that a shattered fracture occurred in these particles prior to the final damage of the composite. Similar results have been reported in TiC-TMCs [29]. This feature fully demonstrates that micro-cracks generate in TiC particles preferentially, and these cracks will expand into matrix at higher deformation. That is to say, the fracture of the composite is controlled by the crack of TiC particles to a great extent.

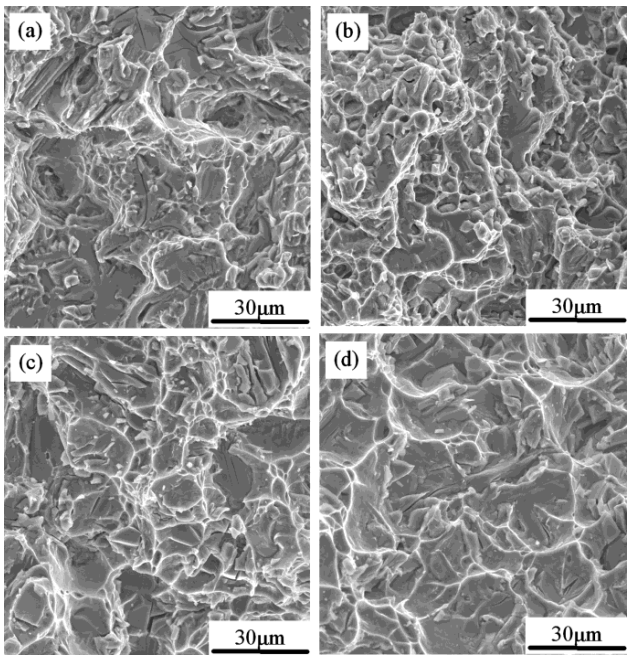

Figure 5. SEM images showing ambient-temperature fracture surfaces of the composite before (**a**) and after heat treatment: (**b**) HT1, (**c**) HT2 and (**d**) HT3.

The basic features on fracture surfaces of heat-treated composites (Figure 5b–d) are similar to those observed in Figure 5a. The difference is that some spheroidised TiC particles with small size did not crack, meaning that interface debonding occurred in these particles during tensile deformation. The number of tearing ridges on fracture surfaces of the composite via HT2 and HT3 heat treatments (Figure 5c,d) increased in comparison with that in Figure 5b. The increased tearing ridges observed in Figure 5c,d are indicative of the good ductility of the composite via HT2 and HT3 heat treatments, consistent with the tensile elongations in Figure 4.

4. Discussion

Several mechanisms of strengthening have been proposed to explain the enhancement of tensile strength of particle-reinforced metal matrix composites [8,9,29,30]. Classical strengthening through load bearing from matrix to particles and matrix strengthening resulting from the change in matrix microstructure are the two important strengthening mechanisms. It has been proved that matrix strengthening makes the largest contribution to the enhancement of the tensile strength of TiC-TMCs [19].

In the view of some researchers, for fully laminar α structure in near-α titanium alloys, the enhancement in YS chiefly comes from the refinement of α phase [31]. Hence, the remarkable refinement of α lath due to HT1 heat treatment attributes to the enhancement of YS of the composite at ambient temperature, since the effective slip length of dislocations in matrix decreases seriously [18]. Sen et al. [32] has reported the similar result in Ti-6Al-4V-B alloys. HT2 and HT3 heat treatments cause the coarsening of α lath and, correspondingly, increase the slip length of dislocations, which directly results in the decrease in YS compared to that in the composite via HT1 at ambient temperature.

In order to further investigate the effect of α lath width on YS of the composite, the variation of YS with the inverse of square root of α lath width is illustrated in Figure 6 according to the Hall–Petch equation. The approximatively linear relationship between YS and the inverse of the square root of α lath width with the correlation coefficient of 0.997 is observable in Figure 6. The same method was used to examine the relationship between YS and α phase size in Ti-6Al-4V-B alloys [32]. This result adequately confirms that the enhanced YS after heat treatment is ascribed to the refinement of α lath.

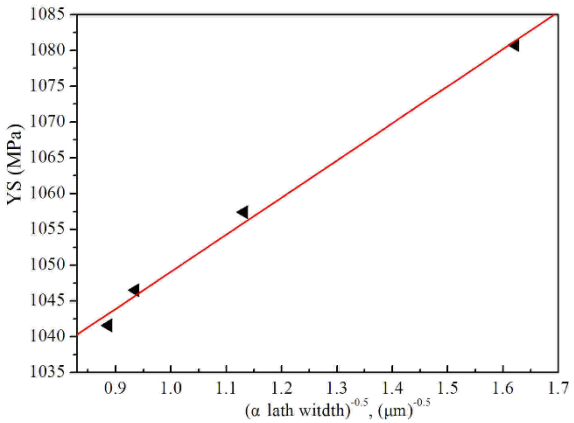

Figure 6. Variation of yield strength (YS) with inverse of square root of α lath width.

As the testing temperature increases to 600 °C, fine grain strengthening can still exert a significant effect on the improvement of tensile strength because the heat-treated composites exhibit higher tensile strength than the as-cast composite (Table 1). With increasing temperature, the degradation in the discrepancy between as-cast tensile strength and heat-treated tensile strength reflects that the role of fine grain strengthening becomes weak. When temperature increases to 700 °C, there is almost no difference in strength between as-cast and heat-treated composites (Table 1). Undoubtedly, the contribution of matrix

strengthening on tensile strength is negligible at this temperature. The variation of matrix strengthening is mainly attributed to the matrix softening at elevated temperatures.

As we know, the refinement of α lath favors the increase in the plasticity in near-α titanium alloys with the fully lamellar structure [33–35]. In addition, spheroidised TiC particles are beneficial for the enhancement in ductility of TiC-TMCs [27]. In fact, the composite via HT1 displays lower elongation compared to as-cast composite at ambient temperature. The presence of hard and brittle TiC particles in matrix can explain this abnormal result because the failure of the composite is dominated by the fracture of TiC particles, which can be confirmed by the results in Figure 5. The stresses acting on TiC particles should increase with the increase in tensile strength of the composite during tensile deformation [36,37]. As the stresses excess their strength, these particles will fracture. The composite via HT1 displays high YS and UTS compared to the as-cast composite. Correspondingly, the local stresses acting on TiC particles increase fast within a small plastic deformation due to the short slip length of dislocations. As a result, fracture probability of TiC particles should be enhanced. More importantly, a large amount of TiC particles will crack within a small plastic deformation, and the cracks in fractured TiC are believed to spread into the matrix rapidly (Figure 5b), which will be bound to decrease the elongation of the composite via HT1.

Based on the analysis above, in TMCs with lamellar structure, α lath size should be controlled strictly to ameliorate the ambient-temperature ductility. Therefore, a new cooling method was employed and performed on the composite in this work with the aim to increase α lath size properly and improve tensile elongation of the composite at ambient temperature. After HT2 and HT3 heat treatments, coarsening of α lath occurs (Figure 3c,d), which results in the degradation of YS. Accordingly, the local stresses acting on TiC particles decrease, and the fracture of TiC particles should be delayed, relatively, responsible for the high ductility of the composite via HT2 and HT3 (Figure 4). With the increase in temperature, the matrix becomes softer and softer, and correspondingly, the influence of the matrix microstructure on elongation is weaker and weaker (Table 1).

Overall, we provide a new heat treatment method to control α phase size in TiC-TMCs with lamellar structure and, thus, control the tensile properties effectively, especially ambient-temperature ductility. As structural materials in the area of aerospace, the room-temperature ductility usually limited the applications of Ti alloy composites. This study provides an efficient method to balance the tensile strength and ductility.

5. Conclusions

In this paper, a new heat treatment was developed and conducted on 10 vol.% TiC/Ti-6Al-3Sn-9Zr-1.5Mo to control the lamellar structure and the effect of α phase size on tensile properties has been discussed. The following conclusions can be drawn:

For as-cast composite, TiC mainly exhibited fine rod and strip shape, and the matrix showed a fully lamellar structure with some extent of basket-weave characteristics. HT1 heat treatment led to the formation of a very fine lamellar microstructure, whereas wider α lath was obtained by HT2 and HT3 heat treatments.

The heat-treated composite with very fine lamellar structure showed high YS and UTS, whereas excellent ductility was obtained in the heat-treated composites via coarse lamellar microstructure at ambient temperature. At elevated temperatures, the matrix microstructure almost had no effect on tensile elongation due to matrix softening. The enhanced YS mainly comes from the refinement of α lath at ambient temperature.

At 600 °C, fine grain strengthening can still exert an obvious influence on tensile strength of the composite. However, with a further increase in temperature, matrix strengthening became weaker and weaker because of matrix softening.

Author Contributions: Conceptualization, D.Z. and J.Q.; data curation, D.Z.; formal analysis, D.Z.; funding acquisition, D.Z., D.D., X.W. and J.Q.; investigation, D.Z., D.D., L.L. and X.W.; methodology, D.D. and L.L.; project administration, D.D. and J.Q.; writing—original draft, D.Z. and D.D. All authors have read and agreed to the published version of the manuscript.

Funding: The research was financially supported by the National Natural Science Foundation of China (Grant Nos. 51801112 and 52071188) and the Natural Science Foundation of Zhejiang Province (Grant Nos. LY18E010003 and LQ20E010003).

Institutional Review Board Statement: Not applicable.

Informed Consent Statement: Not applicable.

Data Availability Statement: The data used to support the findings of this study have not been made available.

Conflicts of Interest: The authors declare no conflict of interest.

References

1. Wang, D.D.; Fan, Q.B.; Gong, H.C.; Zhu, X. Effect of trace carbon on the dynamic compressive properties in the as-cast Ti13V11Cr3Al alloy. *Intermetallics* **2020**, *123*, 106818. [CrossRef]
2. Xie, L.C.; Wang, L.Q.; Zhang, L.C.; Lu, W.J. Editorial: Structure and mechanical properties of titanium alloys and titanium matrix composites (TMCs). *Front. Mater.* **2020**, *7*, 118. [CrossRef]
3. Chen, X.; Huang, L.J.; Jiao, Y.; Wang, S.; An, Q.; Bao, Y.; Gen, L. Mechanisms of oxidation anisotropy between α-Ti (0001) and $(01\bar{1}0)$ crystallographic planes in titanium matrix composites. *Mater. Lett.* **2021**, *286*, 129230. [CrossRef]
4. Fereiduni, E.; Ghasemi, A.; Elbestawi, M. Selective laser melting of hybrid ex-situ/in-situ reinforced titanium matrix composites: Laser/powder interaction, reinforcement formation mechanism, and non-equilibrium microstructural evolutions. *Mater. Des.* **2019**, *184*, 108185. [CrossRef]
5. Li, G.X.; Munir, K.; Wen, C.; Li, Y.C.; Ding, S.L. Machinablility of titanium matrix composites (TMC) reinforced with multi-walled carbon nanotubes. *J. Manuf. Process.* **2020**, *56*, 131–146. [CrossRef]
6. Xu, X.J.; Jin, X.P.; Liu, Z.; Zhang, B.; Zhang, R.K.; Zhuang, Y.; Zhang, P.; Wei, H.B. Influence of large amount Zn on mechanical properties and corrosion resistance of 5083 hot rolled aluminum alloy. *Appl. Phys. A* **2020**, *126*, 713. [CrossRef]
7. Zheng, B.W.; Dong, F.Y.; Yuan, X.G.; Zhang, Y.; Huang, H.J.; Zuo, X.J.; Luo, L.S.; Wang, L.; Su, Y.Q.; Wang, X.; et al. Insights into wear behavior of (TiC + TiB)/TC4 composites against different counterface materials. *Mater. Res. Express* **2019**, *6*, 116584. [CrossRef]
8. Bai, M.W.; Namus, R.; Xu, Y.D.; Guan, D.K.; Rainforth, M.W.; Inkson, B.J. In-situ Ti-6Al-4V/TiC composites synthesized by reactive spark plasma sintering: Processing, microstructure, and dry sliding wear behaviour. *Wear* **2019**, *432*, 202944. [CrossRef]
9. Grützner, S.; Krüger, L.; Schimpf, C.; Radajewski, M.; Schneider, I. Microstructure and Mechanical Properties of In Situ TiB/TiC Particle-Reinforced Ti-5Al-5Mo-5V-3Cr Composites Synthesized by Spark Plasma Sintering. *Metall. Mater. Trans. A* **2018**, *49*, 5671–5682. [CrossRef]
10. He, B.; Lan, J.J.; Yang, G.; Wei, H. Microstructure and wear-resistant properties of in situ TiB-TiC reinforced titanium matrix composites by laser deposition manufacturing. *Rare Met. Mater. Eng.* **2017**, *46*, 3805–3810.
11. Liu, Y.G.; Ru, J.M.; Jiang, Z.; Tabie, V.; Li, C.; Chen, H.; Xu, X.J. Microstructure and oxidation resistance of a Ti-Mo-Nb-Al-Si titanium matrix composite reinforced with in situ TiC prepared by powder metallurgy. *Appl. Phys. A* **2019**, *125*, 791. [CrossRef]
12. Zheng, B.W.; Dong, F.Y.; Yuan, X.G.; Huang, H.J.; Zhang, Y.; Zuo, X.J.; Luo, L.S.; Wang, L.; Su, Y.Q.; Li, W.D.; et al. Microstructure and tribological behavior of in situ synthesized (TiB+TiC)/Ti6Al4V (TiB/TiC=1/1) composites. *Tribol. Int.* **2020**, *145*, 106177. [CrossRef]
13. Ma, X.Z.; Chai, L.H.; Liu, Y.Y.; Cui, Y.P.; Shen, G.L.; Zhang, C.J.; Shu, Q.; Chen, Z.Y. TiB whiskers stimulated the dynamic recrystallization behavior. *J. Alloy. Compd.* **2020**, *812*, 152152. [CrossRef]
14. Yi, M.; Zhang, X.Z.; Liu, G.W.; Wang, B.; Shao, H.C.; Qiao, G.J. Comparative investigation on microstructures and mechanical properties of (TiB+TiC)/Ti-6Al-4V composites from Ti-B_4C-C and Ti-TiB_2-TiC systems. *Mater. Charact.* **2018**, *140*, 281–289. [CrossRef]
15. Zhang, C.J.; Ding, Z.H.; Xie, L.C.; Zhang, L.C.; Wu, L.Z.; Fu, Y.F.; Wang, L.Q.; Lu, W.J. Electrochemical and in vitro behavior of the nanosized composites of Ti-6Al-4V and TiO_2 fabricated by friction stir process. *Appl. Surf. Sci.* **2017**, *423*, 331–339. [CrossRef]
16. Chen, K.P.; Lu, P.; Wang, H.P. Liquid-solid phase transition of Cu-Zr eutectic alloy under microgravity condition. *Acta Phys. Sin.* **2017**, 068101. [CrossRef]
17. Zhang, W.D.; Liu, Y.; Liu, B.; Li, X.F.; Wu, H.; Qiu, J.W. A new titanium matrix composite reinforced with Ti-36Nb-2Ta-3Zr-0.35O wire. *Mater. Des.* **2017**, *117*, 289–297. [CrossRef]
18. Wang, P.P.; Wang, L.Q.; Lu, W.J.; Qin, J.N.; Chen, Y.F.; Zhang, Z.W.; Zhang, D. The effect of heat treatment on mechanical properties of in situ synthesized 7715D titanium matrix composites. *Mater. Sci. Eng. A* **2010**, *527*, 4312–4319. [CrossRef]
19. Qi, J.Q.; Wang, H.W.; Zou, C.M.; Wei, Z.J. Influence of matrix characteristics on tensile properties of in situ synthesized TiC/TA15 composite. *Mater. Sci. Eng. A* **2012**, *553*, 59–66. [CrossRef]
20. Huang, L.J.; Geng, L.; Xu, H.Y.; Peng, H.X. In situ TiC particles reinforced Ti6Al4V matrix composite with a network reinforcement architecture. *Mater. Sci. Eng. A* **2011**, *528*, 2859–2862. [CrossRef]

21. Zhang, Z.G.; Qin, J.N.; Zhang, Z.W.; Chen, Y.F.; Lu, W.J.; Zhang, D. Effect of β heat treatment temperature on microstructure and mechanical properties of in situ titanium matrix composites. *Mater. Des.* **2010**, *31*, 4269–4273. [CrossRef]
22. Qi, J.Q.; Sui, Y.W.; Chang, Y.; He, Y.Z.; Wei, F.X.; Meng, Q.K.; Wei, Z.J. Microstructural characterization and mechanical properties of TiC/near-α Ti composite obtained at slow cooling rate. *Mater. Charact.* **2016**, *118*, 263–269. [CrossRef]
23. Qu, J.P.; Zhang, C.J.; Zhang, S.Z.; Han, J.C.; Chai, L.H.; Chen, Z.Y.; Chen, Y.Y. Relationships among reinforcement volume fraction, microstructure and tensile properties of (TiB_w + TiC_p)/Ti composites after (α + β) forging. *Mater. Sci. Eng. A* **2017**, *701*, 16–23. [CrossRef]
24. Yang, J.H.; Chen, Y.Y.; Xiao, S.L.; Xu, L.J.; Wang, X.P.; Tian, J.; Zhang, D.D.; Zheng, Z.Z. High temperature tensile properties, deformation, and fracture behavior of a hybrid-reinforced titanium alloy composite. *Mater. Sci. Eng. A* **2020**, *788*, 139516. [CrossRef]
25. Qi, J.Q.; Chang, Y.; He, Y.Z.; Sui, Y.W.; Wei, F.X.; Meng, Q.K.; Wei, Z.J. Effects of Zr, Mo and TiC on microstructure and high-temperature tensile strength of cast titanium matrix composites. *Mater. Des.* **2016**, *99*, 421–426. [CrossRef]
26. Qi, J.Q.; Wang, H.W.; Zou, C.M.; Wei, W.Q.; Wei, Z.J. Temperature dependence of fracture behavior of in situ synthesized TiC/Ti-alloy matrix composite. *Mater. Sci. Eng. A* **2011**, *528*, 7669–7673. [CrossRef]
27. Wei, Z.J.; Cao, L.; Wang, H.W.; Zou, C.M. Microstructure and mechanical properties of TiC/Ti-6Al-4V composites processed by in situ casting route. *Mater. Sci. Technol.* **2011**, *27*, 1321–1327. [CrossRef]
28. Zhao, Z.B.; Wang, Q.J.; Hu, Q.M.; Liu, J.R.; Yu, B.B.; Yang, R. Effect of β (110) texture intensity on α-variant selection and microstructure morphology during β→α phase transformation in near α titanium alloy. *Acta Mater.* **2017**, *126*, 372–382. [CrossRef]
29. Hayat, M.D.; Singh, H.; He, Z.; Cao, P. Titanium metal matrix composites: An overview. *Compos. Part A Appl. Sci. Manuf.* **2019**, *121*, 418–438. [CrossRef]
30. Ma, F.C.; Lu, W.J.; Qin, J.N.; Zhang, D. Strengthing mechanisms of carbon element in in situ TiC/Ti_{1100} composites. *J. Mater. Sci.* **2006**, *41*, 5395–5398. [CrossRef]
31. Yang, J.H.; Xiao, S.L.; Chen, Y.Y.; Xu, L.J.; Wang, X.P.; Tian, J.; Zhang, D.D.; Zheng, Z.Z. Microstructure evolution during forging deformation of (TiB + TiC + Y_2O_3)/α-Ti composite: DRX and globularization behavior. *J. Alloy. Compd.* **2020**, *827*, 154170. [CrossRef]
32. Sen, I.; Tamirisakandala, S.; Miracle, D.; Ramamurty, U. Microstructural effects on the mechanical behavior of B-modified Ti-6Al-4V alloys. *Acta Mater.* **2007**, *55*, 4983–4993. [CrossRef]
33. Chandravanshi, V.K.; Sarkar, R.; Kamat, S.V.; Nandy, T.K. Effect of boron on microstructure and mechanical properties of thermomechanically processed near alpha titanium alloy Ti-1100. *J. Alloy. Compd.* **2011**, *509*, 5506–5514. [CrossRef]
34. Bodunrin, M.O.; Chown, L.H.; van der Merwe, J.W.; Alaneme, K.K. Hot working behaviour of experimental Ti-4.5Al-1V-3Fe alloy with initial lamellar microstructure. *Int. J. Adv. Manuf. Technol.* **2020**, *106*, 1901–1916. [CrossRef]
35. Todaro, C.J.; Easton, M.A.; Qiu, D.; Zhang, D.; Bermingham, M.J.; Lui, E.W.; Brandt, M.; StJohn, D.H.; Qian, M. Grain structure control during metal 3D printing by high-intensity ultrasound. *Nat. Commun.* **2020**, *11*, 142. [CrossRef] [PubMed]
36. Nardone, V.C. Assessment of models used to predict the strength of discontinous silicon carbide reinforced aluminum alloys. *Scr. Metall.* **1987**, *21*, 1313–1318. [CrossRef]
37. Nardone, V.C.; Prewo, K.M. On the strength of discontinuous silicon carbide reinforced aluminum composites. *Scr. Metall.* **1986**, *20*, 43–48. [CrossRef]